

Article

Design and Evaluation of a High Temperature Phase Change Material Carnot Battery

Rhys Jacob ^{1,*}  and Ming Liu ²

¹ Forschungszentrum Jülich GmbH, Institute of Energy and Climate Research, Structure and Function of Materials (IEK-2), D-52425 Jülich, Germany

² Future Industries Institute, University of South Australia, Mawson Lakes Boulevard, Mawson Lakes, SA 5095, Australia

* Correspondence: rjacob@fz-juelich.de

Abstract: In the current study, a high temperature thermal storage system with a hybrid of phase change material and graphite as the storage materials is designed and evaluated as to its applicability for use as a utility-scale Carnot battery. The design includes an externally heated liquid sodium tank, which is used as the heat transfer fluid. This is used to charge and discharge the storage system consisting of a graphite storage medium sandwiched by two phase change materials. Finally, electrical generation is by way of a supercritical carbon dioxide Brayton cycle operated at 700 °C. Detailed modelling of these designs was conducted by way of a previously validated numerical model to predict performance metrics. Using the aforementioned designs, a preliminary cost estimate was undertaken to better determine applicability. From these results, it was found that while the graphite system was the most effective at storing energy, it was also the highest cost due to the high cost of graphite. In total, 18 storage tanks containing nearly 17,400 tons of storage material were required to store the 1200 MWh_t required to run the sCO₂ power block for 10 h. Under the study conditions, the cost of a PCM-based Carnot battery was estimated to be \$476/kWh_e, comparable to other storage technologies. Furthermore, it was found that if the cost of the graphite and/or steel could be reduced, the cost of the system could be reduced to \$321/kWh_e.

Keywords: thermal energy storage; Carnot batteries; phase change materials; high temperature



Citation: Jacob, R.; Liu, M. Design and Evaluation of a High Temperature Phase Change Material Carnot Battery. *Energies* **2023**, *16*, 189. <https://doi.org/10.3390/en16010189>

Academic Editors: Karunesh Kant and Atul Sharma

Received: 29 November 2022

Revised: 20 December 2022

Accepted: 20 December 2022

Published: 24 December 2022



Copyright: © 2022 by the authors. Licensee MDPI, Basel, Switzerland. This article is an open access article distributed under the terms and conditions of the Creative Commons Attribution (CC BY) license (<https://creativecommons.org/licenses/by/4.0/>).

1. Introduction

Minimization of the damage caused by climate change remains one of the most pressing issues of the 21st Century. While great effort has been realized in decarbonizing certain areas of the economy (e.g., electrical generation), more work is required [1]. Similarly, other areas (e.g., industry, transport, etc.) are further lacking and require significant investment and support if we are to meet net-zero goals [2,3]. Furthermore, the replacement of traditional energy generators, such as coal and gas (which utilize turbomachinery), with solar photovoltaic or wind turbines, have left some questions about the stability and security of electrical supply [4–7]. Therefore, solutions which are able to be readily dispatched and provide ancillary services (e.g., spinning reserve) are at a premium. One such technology which is able to achieve this are Carnot batteries.

Carnot batteries are a technology which are able to convert electricity (preferable renewable) into heat, which can then be stored thermally. This stored energy can then be reconverted to electricity as it is required [8–10]. Unlike other storage technologies such as electrochemical or hydro-mechanical which have significant environmental impact due to their need of critical materials [11] or land changes [12], respectively, Carnot batteries typically use low-cost, abundant materials and can be deployed in almost all locations. Previous studies have also shown that these systems are able to compete financially with the aforementioned storage technologies [8,9,13,14], making them a promising choice for energy storage applications in a highly renewable system.

Currently, most deployed or proposed Carnot batteries utilize sensible thermal storage (i.e., raising the temperature of a material to achieve energy storage) [15], although research has shown how thermal storage systems can benefit from the use of phase change materials (PCMs) to reduce the cost of the system and to increase storage efficiency [16–21]. For example, Mathur et al. (2014) [16] investigated the cost reduction in using encapsulated PCMs as a high temperature storage option for concentrated solar power (CSP) plants. The cost of a traditional two-tank system and an encapsulated phase change material (EPCM) system was compared to best illustrate the cost reduction potential of the newly developed system. It showed that for a given set of assumptions, the 3-PCM cascaded EPCM system was estimated to be \$16/kWh, a saving of 40% over the traditional two-tank system. Further cost reductions were found for EPCM hybrid systems (e.g., thermal energy storage (TES) systems with both solid and PCM fillers) in research by Zhao et al. (2016) [17] who investigated several multilayer solid-PCM systems and the cost of such systems. Each system was optimized with respect to the design considerations and compared to a molten salt thermocline system and a two-tank molten salt system. Cost reductions of $\approx 23\%$ and $\approx 38\%$ were realized when compared to sensible thermocline and two-tank molten salt systems, respectively. Albert et al. (2022) [18] specifically investigated the impact of latent heat storage on the round-trip efficiency of a pumped thermal energy storage (PTES) system. In this system, the storage was described as a packed bed system with encapsulated PCM being added to maintain a high temperature output during discharging. The authors found that in adding these encapsulated materials to the magnetite system, the round-trip efficiency reached 80%, very close to the theoretically predicted limit. Due to this, the levelized cost of storage (LCOS) was reduced from 0.11 €/kWh to 0.07 €/kWh without and with latent heat storage, respectively. Similar efficiency increases and cost reductions have also been found for shell-and-tube configurations, with research by Liu et al. (2020) [19] suggesting a 5-PCM cascade system would be cheaper than a solid graphite system while a hybrid system (2-PCM and graphite) would be cheaper and more effective than either the 5-PCM cascade or graphite-only system. Similar trends were observed by Jacob et al. (2021) [20], who showed that cascaded PCM systems would be cheaper than two-tank liquid sodium or graphite-only systems, although a two-tank molten chloride system would be cheaper still. However, when the cost of integration into the CSP plant was included, the cost of the 2-PCM/graphite hybrid system resulted in the lowest costs.

While PCMs have been shown to be promising, their use in Carnot batteries is currently not well studied, especially for shell-and-tube designs. Therefore, the current study investigates a PCM-based Carnot battery design for its efficiency and cost as a way of evaluating the potential feasibility of this storage configuration for utility-scale applications. In doing so, researchers and technology developers can better understand its role in the energy transition and provide insights for how Carnot batteries may be improved.

2. Materials and Methods

The following section outlines the methodology of the system design and material selection.

2.1. Numerical Modelling

The performance of the system was numerically simulated for which a design to meet the stated objectives could be determined. The performance of the charge tank and power block were fixed using previously determined parameters, while the performance of the TES system was determined using a 2-D model. The results of this study were then used to determine the cost of the system (Section 2.4).

2.1.1. Liquid Sodium Charge Tank

The charging of the PCM-TES system is to take place by way of an electrically charged liquid sodium tank. This involves the placement of resistive elements to generate heat. As liquid sodium has a high thermal conductivity [22], it can be assumed that the temperature

of the tank is uniform. The volume of the charge tank can be determined by the volume of sodium required to fill the shell and tubes of the PCM storage tank, plus a 15% buffer to account for further connection piping and minimum pumping head (Equations (1)–(3)).

$$V_{Na} = ((\#_{tube} * V_{tube} + 2 * V_{header}) * \#_{tank}) * 1.15 \quad (1)$$

$$V_{tube} = \pi * r_{tube}^2 * L_{tube} \quad (2)$$

$$V_{header} = 1.05 * \left(\frac{\frac{4}{3}(d_{tank} + w_{tank})^3}{16} - \frac{\frac{4}{3}(d_{tank})^3}{16} \right) \quad (3)$$

2.1.2. Thermal Storage Performance

The numerical modelling performed in the current study is based on previous work by Tay et al. (2018) [23] and Liu et al. (2020) [19] and is briefly presented here for reference. For more detail, including validation, readers are directed to the work of Tay et al. (2018) [23] and Liu et al. (2020) [19].

As shown in Figure 1a, the shell-and-tube TES system consists of a group of parallel tubes inside a cylindrical tank. The center-to-center distance between two adjacent tubes is $2r_o$ in Figure 1c. The PCM is filled in the shell space between tubes, while the HTF flows inside the inner tubes and exchanges energy with the PCM by heat convection and heat conduction through the tube wall. To simplify the mathematical model, this physical system to be analyzed can be represented by one unit in Figure 1b with adiabatic condition at the outer PCM surface, assuming the flow is equally distributed in each tube and the cylindrical tank is well insulated thus no heat loss through the TES system. The shell-and-tube arrangement is the most promising for a latent heat storage system requiring high efficiency with a minimum volume [24] and sophisticated experience exists in the manufacturing sector to build shell-and-tube heat exchangers.

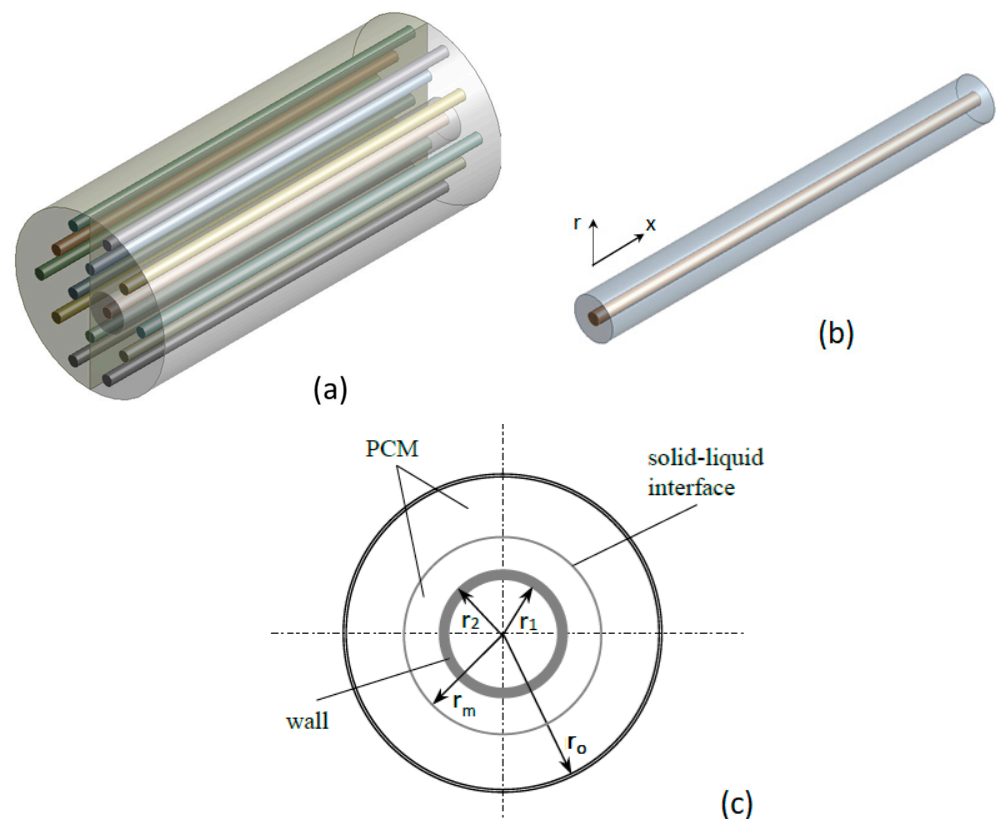


Figure 1. Schematic diagram of: (a) a shell-and-tube TES system; (b) one modelled storage unit and (c) top view of one cross-section of the modelled unit.

A two-dimensional (2-D) unsteady state numerical model was developed to study the thermal performance of one shell-and-tube unit by the co-authors in Tay et al. (2018) [23], which consists of 2-D conduction heat transfer models along both the x - and r -direction in the domains of PCM annulus and tube wall and a 1-D convective heat transfer model in the HTF along the x -direction. The enthalpy method developed by Voller (1990) [25] was employed to solve the phase change problem, assuming that the PCM solid-liquid interface is axisymmetric around the x -axis and the radius of this interface (r_m as shown in Figure 1c) varies along the x -axis. The heat conduction is the dominant heat transfer in the PCM and the effect of natural convection in liquid PCM is included in the heat conduction equation by using an effective thermal conductivity (k_e), which is defined by:

$$k_e/k_l = \max(1, CRa^n) \quad (4)$$

where Ra is the Rayleigh number and C and n are constants, which have been determined by the experiment to be 0.18 and 0.25 [23]. Employing an effective thermal conductivity is a common approach in numerical modelling to account for the acceleration effect of natural convection on the heat transfer [26].

In Tay et al.'s work (2018) [23], the developed model was validated against the experimental results using water as a PCM. The model was further verified by Liu et al. (2020) [19] using the simulated results by a commercial computational fluid dynamics package, ANSYS FLUENT 17, which has been approved to be an accurate tool to design the TES systems with inorganic salts as PCMs under high-temperature conditions.

2.1.3. Brayton Cycle Output

In the current study, a simple closed-loop Brayton cycle (Figure 2) is employed, where, under the conditions of the current study, the efficiency of the cycle is 46% and the efficiency of the primary heat exchanger is 95% [27].

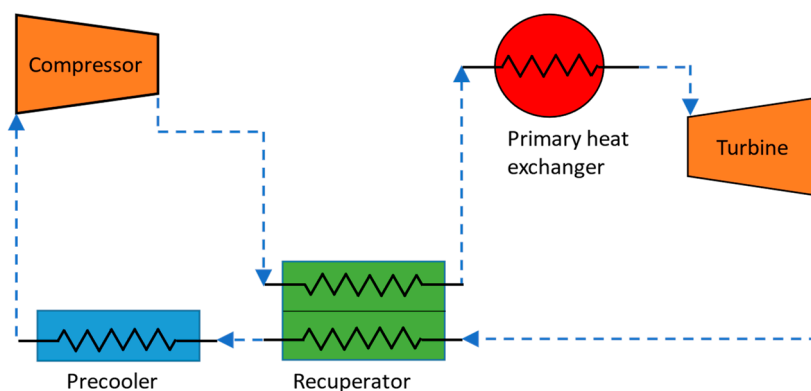


Figure 2. Simple closed-loop Brayton Cycle.

2.2. Materials Studied

For the current study, liquid sodium has been chosen as the heat transfer fluid (HTF) owing to its favorable heat capacity, thermal conductivity, and relatively low price [22,28]. Under similar conditions, it has been shown that a 2-PCM/graphite hybrid would result in the highest storage efficiency and lowest cost [19,20], therefore, this configuration was chosen for the thermal storage. The PCMs chosen include a binary potassium-sodium carbonate eutectic (47.19 wt.% Na_2CO_3), and a ternary sodium carbonate, sodium chloride, potassium chloride eutectic (41.6 wt.% Na_2CO_3 , 33.0 wt.% KCl). Similar to the aforementioned studies, the PCM occupies approximately 10% of the system by volume. Lastly, electrical generation by way of a Brayton cycle with supercritical carbon dioxide (sCO_2) as the working fluid (WF) was considered. Table 1 summarizes the thermophysical properties of the materials used in the current study.

Table 1. Thermophysical Properties of Studied Materials.

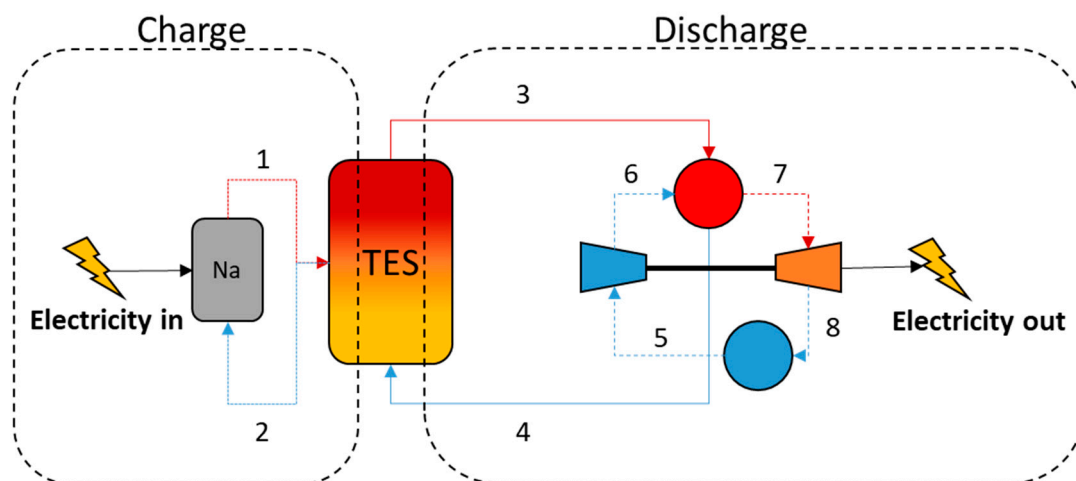
Property	HTF-Liquid Sodium (@700 °C) ¹	PCM 1-PCM710 ²	Graphite ²	PCM 2-PCM569 ²	WF-sCO ₂ (@700 °C, 20 MPa) ³
Specific Heat (J/kg·K)	1251.38	1540 [s] 1500 [l]	1600	1340 [s] 1410 [l]	1273.1
Melting Point (°C)	-	705.8	-	569	-
Latent Heat (J/kg)	-	144,900	-	249,600	-
Thermal Conductivity (W/m·K)	53.42	0.6 [s] 0.5 [l]	50	0.6 [s] 0.5 [l]	0.072
Density (kg/m ³)	792	2000	1800	2000 [s] 1700 [l]	106
Viscosity (Pa·s)	0.0002	0.007	-	0.004	0.0042

[s] solid; [l] liquid; ¹ <https://doi.org/10.1016/j.solener.2012.05.001> (accessed on 23 December 2022); ² <https://doi.org/10.1016/j.renene.2019.11.115> (accessed on 23 December 2022); ³ NIST Standard Reference Database 12.

2.3. Design Conditions

The current study considers a utility-scale Carnot battery as the design case with an average charge capacity of 200 MW_t, an average discharge capacity of 120 MW_t, and a total storage capacity of 1200 MWh_t. In this scenario, the charge cycle is assumed to last for six hours, discharging lasts for 10 h, and standby is for eight hours. The time of each occurrence will be dictated by the availability and cost of electricity, but as to how that is achieved is outside the scope of the current paper. During the charge or discharge cycle, it is assumed that the input/output is at full capacity.

The studied Carnot configuration contains four main elements: the liquid sodium charge tank, the thermal storage system, the HTF-WF (primary) heat exchanger, and the Brayton cycle power block (Figure 3).

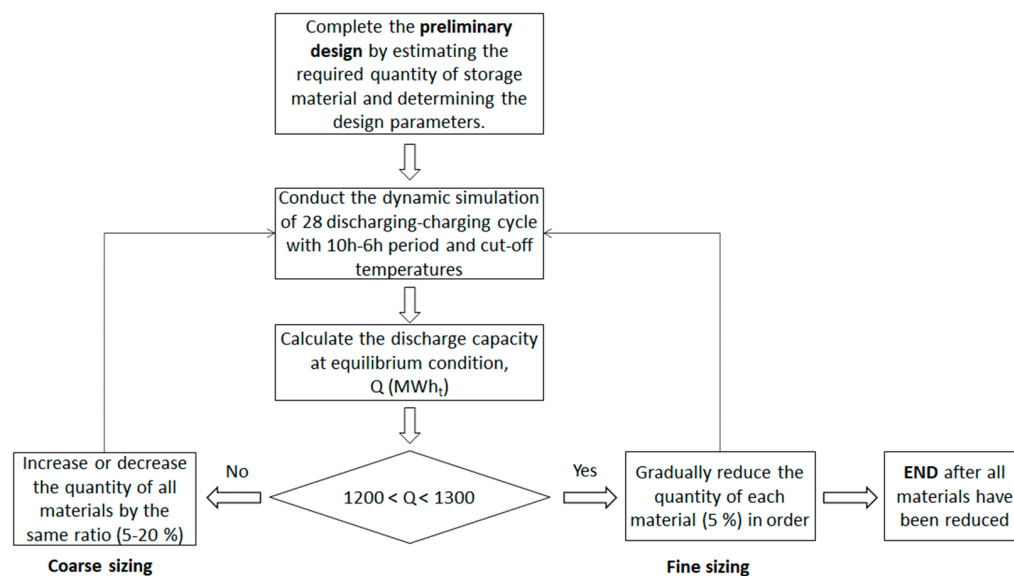
**Figure 3.** Outline of a Cascaded PCM TES Carnot Battery with a sCO₂ Brayton Cycle.

During charging, resistive elements are used to heat the tank of liquid sodium to 750 °C, which, in turn, is used to heat the PCM or graphite storage up to 750 °C. Once charged, the colder liquid sodium (540 °C) can be reheated using the energy stored in the TES system to run the sCO₂ Brayton cycle. Under these conditions the cut-off temperature from the TES to the heat exchanger is 700 °C, while the turbine inlet temperature is 690 °C. The as-stated design conditions are summarized in Table 2, below.

Table 2. Operating Conditions of Analysed Carnot Battery.

Stream #	Fluid	Temperature (°C)	Pressure (Bar)
1	Liquid Sodium	750	1
2	Liquid Sodium	540–580	1
3	Liquid Sodium	700–750	1
4	Liquid Sodium	540	1
5	sCO ₂	520	80
6	sCO ₂	520	200
7	sCO ₂	690	200
8	sCO ₂	690	80

The methodology and procedure to size a PCM or graphite hybrid TES system has been explained in Liu et al. (2021) [21], as summarized in the flow chart in Figure 4. A tube size of DN 8 Sch 40S (OD: 13.72 mm; ID: 9.24 mm) and a tube spacing of 56.2 mm and 116.2 mm in PCM and graphite, respectively, were employed since these parameters have been verified to achieve an improved performance by Liu et al. (2021) [21]. Similar to Liu et al. (2021) [21], the tank wall thickness was 12 mm.

**Figure 4.** Flow chart of the design and sizing procedure.

2.4. Economic Assessment

The cost of the system was determined by estimating the material requirements for each design to meet the stated energy storage power and capacity. This methodology has previously been used to estimate the cost of encapsulated PCM storage systems [29,30] and other PCM shell-and-tube systems [20,21,31]. In particular, the current study uses the cost estimation method developed by Liu et al. (2021) [21] for TES costs, and readers are referred to the source material for the methodology and important equations. Cost information on other components, such as the resistive heater and sCO₂ power block, have been sourced from [27,32,33] and are summarized in Equations (5) and (6).

$$C_{rh} = 75,000 * P_{rh}^{0.9} \quad (5)$$

$$C_{PB} = 942 * P_{PB} \quad (6)$$

where C_{rh} and P_{rh} are the cost (\$) and power (MW) of the resistive elements, respectively and C_{PB} and P_{PB} are the cost of the power block (\$) and power (kW_e), respectively.

Material costs and assumptions were assigned based on average bulk costs of raw materials from various vendors and/or literature values [29,31,34] and is summarized in

Table 3. It should be noted that these costs are bulk material costs averaged across a range of vendors (Appendix A) and locations and may not reflect true system cost, but ultimately provide data from which a comparison of systems can be made.

Table 3. Material Costs in the Current Study.

Material	Cost (\$US)	Material	Cost (\$US)	Material	Cost (\$US)
HTF	\$2.4/kg ⁴	PCM710	\$0.5/kg	Graphite	\$6/kg ⁵
PCM569	\$0.4/kg	Vessel Material	\$6.6/kg ⁶	Tube Material	\$6.4/kg ⁷
External Insulation	\$256/m ²	Foundation and Footings	\$1320/m ²	Installation	30% Material Cost

⁴ <https://www.metal.com/Other-Minor-Metals/201102250465> (accessed on 14 September 2022);

⁵ https://www.alibaba.com/product-detail/wholesale-EDM-Graphite-brick-and-graphite_60699534142.html?spm=a2700.galleryofferlist.normal_offer.d_title.479085efbVkwYc (accessed on 14 September 2022);

⁶ <https://mepsinternational.com/gb/en/products/world-stainless-steel-prices> (Hot Rolled Plate 316) (accessed on 14 September 2022); ⁷ <https://mepsinternational.com/gb/en/products/world-stainless-steel-prices> (Cold Rolled Coil 316) (accessed on 14 September 2022).

3. Results and Discussion

3.1. Sizing the TES System

The results of sizing the PCM/graphite hybrid system are summarized in Table 4. After eight consecutive discharging-charging cycles, the discharging-charging process reaches an equilibrium condition, meaning the difference of state of charge at the end of both discharging and charging between the 8th cycle and the cycles afterward is less than 1% [19]. The temperature of the HTF at the outlet of TES system and the heat transfer rate during both the discharging and charging process at equilibrium condition are plotted in Figure 5. The designed hybrid system is capable of providing a storage capacity of 1235 MWh_{th}, with an average discharging and charging rate of 123.5 MW_{th} and 201.8 MW_{th} over a 10-h discharging period and 6-h charging period, respectively, meeting the design criterion.

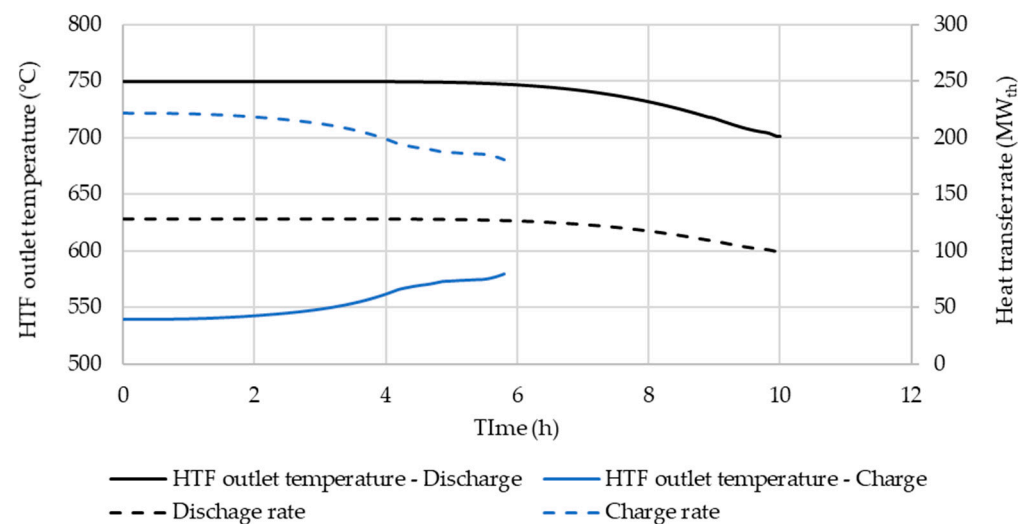


Figure 5. HTF outlet temperature and heat transfer rate for charging and discharging processes.

Table 4. Design specifications of the hybrid TES system.

Storage Material	Required Quantity (Tonnes)	Discharge Capacity (MWh _{th})	Energy Density (KWh _{th} /Tonne)	Storage Effectiveness	No. of Tubes	Total Tube Length (m)	Tank Size [r × L] (m × m)	No. Tanks
PCM710	912	25	27.5	21.3%	8135	21.6	2.82 × 7.20	3
graphite	15,574	1153	74.1	79.3%		96.0	5.82 × 8.00	12
PCM569	912	57	62.2	41.2%		21.6	2.82 × 7.20	3
total	17,398	1235	71.0	72.3%		139.2		18

3.2. Economic Evaluation

The cost of the system is based on the individual cost of the liquid sodium charge tank (including electrical elements), the cost of the storage system, and the cost of the power block.

3.2.1. Liquid Sodium Charge Tank

The cost of the liquid sodium charge tank can be calculated using the same methodology for estimating the cost of the storage tanks. Additional costs for the sodium to fill the system and the electrical elements are also included. Using Equations (1)–(3), the volume of the liquid sodium in the system was estimated to be 100.5 m³, with a mass of 78.6 tons. Assuming a tank aspect ratio (H/D) of 2:1, the dimensions of the charge tank are 4 × 8 m (ID × h), with a wall thickness of 6 mm. A cost breakdown of the liquid sodium charge tank costs can be found in Table 5 and Figure 6.

From Figure 6, it can be seen that the cost of the heaters dominates the cost of the system while the cost of the liquid sodium in the system is not insignificant. Installation of the system is also expected to be a significant expense.

Table 5. Cost of Liquid Sodium Charge Tank Components.

Parameter	Value	Parameter Cost	Total Cost	% Total Cost
Liquid Sodium Tank-total	-	Vessel + insulation + foundation	\$85,183	1%
Liquid Sodium Tank-vessel	6.0 t	\$6.60/kg	\$39,407	46%
Liquid Sodium Tank-insulation	113.6 m ²	\$256/m ²	\$29,088	34%
Liquid Sodium Tank-foundation	12.6 m ²	\$1320/m ²	\$16,687	20%
Resistive Heaters	200 MW _e	Equation (5)	\$8,830,560	75%
Liquid Sodium Installation	78.6 t	\$2.4/kg	\$188,740	2%
	-	30% direct	\$2,731,345	23%
TOTAL	-	-	\$11,835,827	100%

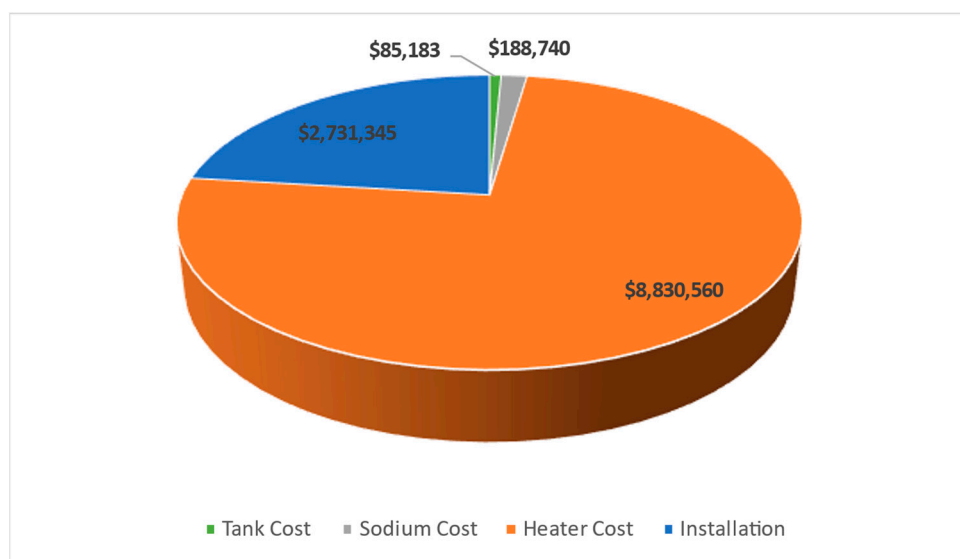


Figure 6. Cost Breakdown of the Liquid Sodium Charge Tank.

3.2.2. Thermal Storage System

Using the storage system sizes given in Table 4, it is possible to estimate the cost of the thermal storage system. A summary of the calculated costs and a breakdown of each system is shown in Table 6 and Figure 7.

From Table 6 it can be seen that the total storage costs are dominated by the cost of the graphite system. While it is expected given that this system stores the majority of the energy (93%), the cost of energy storage is also the highest (\$115.49/kWh_t). Looking at Figure 7, it can be seen that this is due to the very high cost of graphite used in the current study. For the PCM systems, the cost breakdown shows approximately equal proportions for material cost, containment costs, tube costs, and installation. Of the studied systems, the PCM569 system is the most cost effective due to the relatively low storage media cost coupled with a higher storage effectiveness (41.2%), which is the disadvantage of the PCM710 system.

Table 6. Summary of Thermal Storage System Costs.

Parameter	System 1-PCM710	System 2-Graphite	System 3-PCM569	TOTAL
Storage Material Cost	\$456,000	\$93,444,000	\$364,800	\$94,264,800
System Containment Cost-TOTAL	\$597,510	\$5,793,056	\$597,510	\$6,988,075
System Containment Cost- Tank Material	\$287,949	\$2,404,951	\$287,949	\$2,980,849
System Containment Cost- Insulation	\$161,526	\$2,033,215	\$161,526	\$2,356,268
System Containment Cost- Foundation	\$148,034	\$1,354,890	\$148,034	\$1,650,959
Tube Material Cost	\$717,725	\$3,189,889	\$717,725	\$4,625,340
Installation	\$531,370	\$30,728,084	\$504,010	\$31,763,464
TOTAL	\$2,302,605	\$133,155,029	\$2,184,045	\$137,641,679
TOTAL (\$/kWh_t)	\$92.10	\$115.49	\$38.32	\$111.45

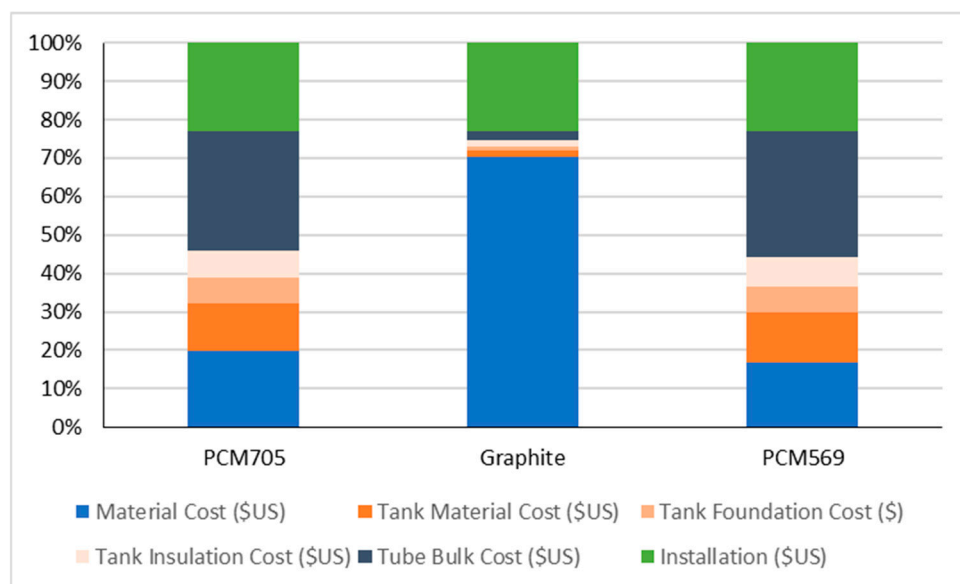


Figure 7. Cost Breakdown of Studied Thermal Storage Systems.

3.2.3. Power Block Costs

Using Equation (6), the cost of the power block was estimated to be \$113,040,000. Under the stated conditions, the power block is expected to have a discharge capacity of 55.2 MW_e for 10 h (552 MWh_e).

3.2.4. Total System Cost

Using the results from Sections 3.2.1–3.2.3, the cost of the Carnot battery could be estimated. The total cost of the system was calculated to be \$262.5 million, of which the thermal storage and power block were 52% and 43% of the costs, respectively. At this cost, the cost of power and energy were calculated as \$4756/kW_e and \$476/kWh_e, respectively, which compare well with the energy storage costs of other electricity storage options, such as Li-ion batteries.

3.3. Cost Sensitivity

Overall, the costs of the thermal storage system are much higher than previously evaluated systems (e.g., [20,21]) due to the high cost of graphite and steel assumed in the current study. However, there is potential for these costs to be reduced, e.g., through the use of lower quality graphite (assuming the properties are largely unaffected) or a return to lower stainless-steel costs (as seen prior to 2019). To estimate what the impact of these price changes on the cost of the storage system would be, an investigation was carried out to calculate the cost of the thermal storage system with a graphite cost of \$2/kg and a stainless-steel cost of \$3.5/kg. The results from this investigation are given in Figure 8.

From Figure 8 it can be seen that the cost of the system is most affected by the cost of the graphite. In reducing the cost of graphite to \$2/kg, the cost of the storage system reduces by 2.4 times. Approximately, for every \$1/kg decrease in the graphite cost, the cost of the storage system reduces by 15–20%. However, while the lowering of the steel cost has some positive impact on reducing the system cost, the benefit is marginal. Therefore, research should be focused on successfully using lower quality graphite or alternate storage materials to reduce the cost of the thermal storage system.

If these costs are instead used for the Carnot battery system, the cost of power and energy reduces to \$3206/kW_e and \$321/kWh_e, respectively. It should also be noted that the system is not fully optimized for the design conditions and that better matching of the storage materials and capacity to the design conditions would further reduce the cost of storage and the system in general.

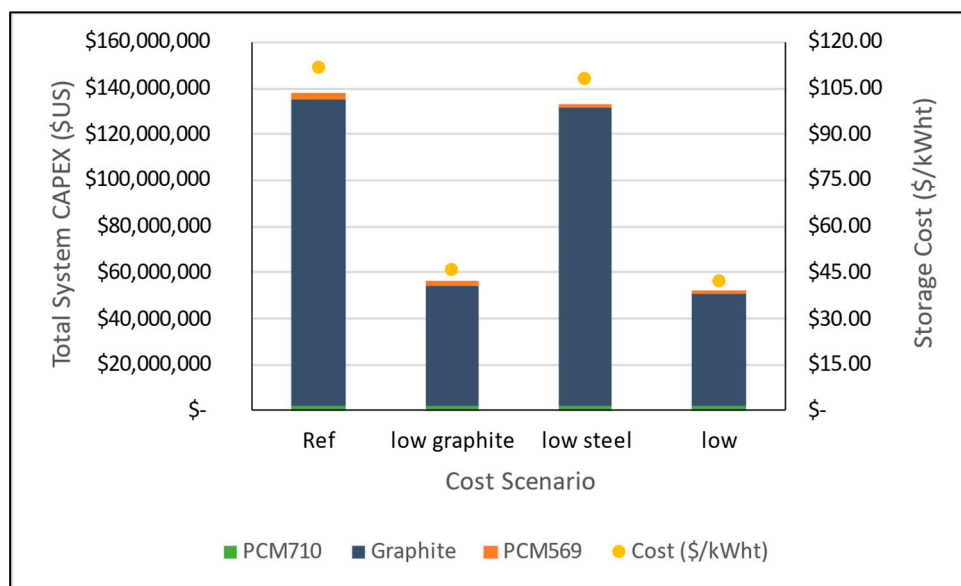


Figure 8. CAPEX Variation with Material Costs.

4. Conclusions

The current study preliminarily investigates the techno-economic feasibility of using PCM-based Carnot batteries for utility-scale energy storage. The system was composed of three main components: the liquid sodium charge tank, the thermal storage system, and the $s\text{CO}_2$ power block. Using a previously validated numerical model, the design of a suitable thermal storage system could be established. From this analysis, it was found that the graphite system, while being the most effective at storing energy, also had the highest cost due to the high cost of graphite. In total, 18 storage tanks containing nearly 17,400 tons of storage material were required to store the 1200 MWh_t required to run the $s\text{CO}_2$ power block for 10 h. Under the study conditions, the cost of a PCM-based Carnot battery was estimated to be $\$476/\text{kWh}_e$, comparable to other storage technologies. Furthermore, it was found that if the cost of the graphite and/or steel could be reduced, the cost of the system could be reduced to $\$321/\text{kWh}_e$.

Author Contributions: All authors contributed equally to all sections of the paper including analysis, writing, and editing. All authors have read and agreed to the published version of the manuscript.

Funding: This research was funded by the Alexander von Humboldt Foundation and the Department of Industry, Science, Energy and Resources (Australia) through Australia India Strategic Research Fund (AIRXII000124).

Data Availability Statement: Provided upon request.

Acknowledgments: Rhys Jacob would gratefully like to acknowledge the Alexander von Humboldt Foundation for providing funding to undertake this work.

Conflicts of Interest: The authors declare no conflict of interest. Additionally, the funders had no role in the design of the study; in the collection, analyses, or interpretation of data; in the writing of the manuscript; or in the decision to publish the results.

Nomenclature

C	constant in Equation (4)	
C_o	Cost/CAPEX	\$
c_p	specific heat capacity	$\text{J}/(\text{kg}\cdot\text{K})$
d	diameter	m
h	height	m
ΔH_m	latent heat of fusion	J/kg

k	thermal conductivity	$W/(m \cdot K)$
L	length	m
M	mass	kg or <i>tonne</i>
\dot{m}	HTF mass flow rate	kg/s
n	constant in Equation (2)	
Nu	Nusselt number	
P	power	kW/MW
Pr	Prandtl number	
Q	energy	$MWhr$
r	radius coordinate	m
Ra	Rayleigh number	
Re	Reynolds number	
t	time	s
Δt	time step	s
T	temperature	$^{\circ}C$
T_m	melting point of PCM	$^{\circ}C$
V	volume	m^3
w	Wall thickness	mm or m
x	axial coordinate	m
X^+	Dimensionless axial coordinate	
#	number	
<u>Greek symbols</u>		
α	thermal diffusivity	m^2/s
ρ	density	kg/m^3
μ	dynamic viscosity	$kg/m \cdot s$
β	Thermal expansion	$1/K$
<u>Subscripts</u>		
e	effective	
$header$	header	
in	inlet	
l	liquid	
Na	sodium	
out	outlet	
PB	power block	
rh	resistive heater	
s	solid	
$tank$	tank	
$tube$	tube	
w	tube wall	

Appendix A

Bulk Material Costs.

Table A1. Bulk Vendor Costs for Na_2CO_3 .

Low Estimate (\$/t)	High Estimate (\$/t)	Average (\$/t)	Accessed	Reference
380	580	480	14 September 2022	https://www.alibaba.com/product-detail/Industrial-Standard-Packaging-25KG-Sodium-Carbonate_1600606722357.html?spm=a2700.7724857.0.0.5f3c393dhnJDHt&s=p
220	240	230	14 September 2022	https://www.alibaba.com/product-detail/soda-ash-dense-sodium-carbonate_60220579681.html?spm=a2700.7724857.0.0.5f3c393dhnJDHt
260	300	280	14 September 2022	https://www.alibaba.com/product-detail/China-99-2-Double-Ring-GGG_1600447288788.html?spm=a2700.7724857.0.0.5f3c393dhnJDHt

Table A2. Bulk Vendor Costs for K₂CO₃.

Low Estimate (\$/t)	High Estimate (\$/t)	Average (\$/t)	Accessed	Reference
700	950	825	14 September 2022	https://www.alibaba.com/product-detail/Factory-supply-Fertilizer-Food-Grade-99_1600104932270.html?spm=a2700.7724857.0.0.70894047syRmTC
100	200	150	14 September 2022	https://www.alibaba.com/product-detail/Potassium-Carbonate-K2CO3-_50011239553.html?spm=a2700.7724857.0.0.70894047syRmTC
500	1500	1000	14 September 2022	https://www.alibaba.com/product-detail/Low-price-tech-grade-food-grade_62139621813.html?spm=a2700.7724857.0.0.70894047syRmTC

Table A3. Bulk Vendor Costs for KCl.

Low Estimate (\$/t)	High Estimate (\$/t)	Average (\$/t)	Accessed	Reference
400	800	600	14 September 2022	https://www.alibaba.com/product-detail/Wholesale-Industrial-Grade-Potassium-Chloride-Bulk_1600534320946.html?spm=a2700.7724857.0.0.3a50720efrKaDR
700	850	775	14 September 2022	https://www.alibaba.com/product-detail/Potassium-Chloride-KCL-99-0-_60201681083.html?spm=a2700.7724857.0.0.3a50720efrKaDR
780	830	805	14 September 2022	https://www.alibaba.com/product-detail/China-High-Purity-Min-99-5_1600324386980.html?spm=a2700.7724857.0.0.3a50720efrKaDR

Table A4. Bulk Vendor Costs for NaCl.

Low Estimate (\$/t)	High Estimate (\$/t)	Average (\$/t)	Accessed	Reference
55	110	82.5	14 September 2022	https://yifengtuo.en.made-in-china.com/product/WFwfacSGXTRb/China-Supply-Industrial-Sodium-Chloride-Price-CAS-7647-14-5.html
77	121	99	14 September 2022	https://yaoshengcompany.en.made-in-china.com/product/zwhAsqfoAMYH/China-From-Factory-Price-of-Sodium-Chloride-Industry-Grade-99-.html
55	165	110	14 September 2022	https://yaoshengcompany.en.made-in-china.com/product/KFqaCObMcoRX/China-Factory-Price-of-Sodium-Chloride-Industry-Grade-99-.html

References

- IEA. *Tracking Power 2021*; IEA: Paris, France, 2021. Available online: <https://www.iea.org/reports/tracking-power-2021> (accessed on 8 September 2022).
- IEA. *Tracking Industry 2021*; IEA: Paris, France, 2021. Available online: <https://www.iea.org/reports/tracking-industry-2021> (accessed on 8 September 2022).
- IEA. *Tracking Transport 2021*; IEA: Paris, France, 2021. Available online: <https://www.iea.org/reports/tracking-transport-2021> (accessed on 8 September 2022).
- Rawat, M.S.; Vadhera, S. A Comprehensive Review on Impact of Wind and Solar Photovoltaic Energy Sources on Voltage Stability of Power Grid. *J. Eng. Res.* **2019**, *7*, 178–202.
- Zhu, M. The impact of new energy generation on grid frequency. *AIP Conf. Proc.* **2019**, *2066*, 020044. [CrossRef]
- Johnson, S.C.; Rhodes, J.D.; Webber, M.E. Understanding the impact of non-synchronous wind and solar generation on grid stability and identifying mitigation pathways. *Appl. Energy* **2020**, *262*, 114492. [CrossRef]

7. Swiss, R.E. Changing Energy Mix and Its Impact on Grid Stability. 2021. Available online: <https://corporatesolutions.swissre.com/dam/jcr:81569f57-635a-4450-93e3-466990694643/changing-energy-mix-and-its-impact-on-grid-stability.pdf> (accessed on 8 September 2022).
8. Benato, A.; Stoppato, A. Pumped Thermal Electricity Storage: A technology overview. *Therm. Sci. Eng. Prog.* **2018**, *6*, 301–315. [[CrossRef](#)]
9. Frate, G.F.; Ferrari, L.; Desideri, U. Critical review and economic feasibility analysis of electric energy storage technologies suited for grid scale applications. *E3S Web Conf.* **2019**, *137*, 01037. [[CrossRef](#)]
10. Dumont, O.; Frate, G.F.; Pillai, A.; Lecompte, S.; De paepe, M.; Lemort, V. Carnot battery technology: A state-of-the-art review. *J. Energy Storage* **2020**, *32*, 101756. [[CrossRef](#)]
11. IEA. *The Role of Critical Minerals in Clean Energy Transitions*; IEA: Paris, France, 2021. Available online: <https://www.iea.org/reports/the-role-of-critical-minerals-in-clean-energy-transitions> (accessed on 8 September 2022).
12. EIA. Hydropower Explained- Hydropower and the Environment. 2021. Available online: <https://www.eia.gov/energyexplained/hydropower/hydropower-and-the-environment.php> (accessed on 8 September 2022).
13. Smallbone, A.; Jülch, V.; Wardle, R.; Roskilly, A.P. Levelised Cost of Storage for Pumped Heat Energy Storage in comparison with other energy storage technologies. *Energy Convers. Manag.* **2017**, *152*, 221–228. [[CrossRef](#)]
14. Georgiou, S.; Shah, N.; Markides, C. A thermo-economic analysis and comparison of pumped-thermal and liquid-air electricity storage systems. *Appl. Energy* **2018**, *226*, 1119–1133. [[CrossRef](#)]
15. Novotny, V.; Basta, V.; Smola, P.; Spale, J. Review of Carnot Battery Technology Commercial Development. *Energies* **2022**, *15*, 647. [[CrossRef](#)]
16. Mathur, A.; Kasetty, R.; Oxley, J.; Mendez, J.; Nithyanandam, K. Using Encapsulated Phase Change Salts for Concentrated Solar Power Plant. *Energy Procedia* **2014**, *49*, 908–915. [[CrossRef](#)]
17. Zhao, B.-C.; Cheng, M.-S.; Liu, C.; Dai, Z.-M. Thermal performance and cost analysis of a multi-layered solid-PCM thermocline thermal energy storage for CSP tower plants. *Appl. Energy* **2016**, *178*, 784–799. [[CrossRef](#)]
18. Albert, M.; Ma, Z.; Bao, H.; Roskilly, A.P. Operation and performance of Brayton Pumped Thermal Energy Storage with additional latent storage. *Appl. Energy* **2022**, *312*, 118700. [[CrossRef](#)]
19. Liu, M.; Riahi, S.; Jacob, R.; Belusko, M.; Bruno, F. Design of sensible and latent heat thermal energy storage systems for concentrated solar power plants: Thermal performance analysis. *Renew. Energy* **2020**, *151*, 1286–1297. [[CrossRef](#)]
20. Jacob R.Riahi, S.; Liu, M.; Belusko, M.; Bruno, F. Technoeconomic Impacts of Storage System Design on the Viability of Concentrated Solar Power Plants. *J. Energy Storage* **2021**, *34*, 101987. [[CrossRef](#)]
21. Liu, M.; Jacob, R.; Belusko, M.; Riahi, S.; Bruno, F. Techno-economic analysis on the design of sensible and latent heat thermal energy storage systems for concentrated solar power plants. *Renew. Energy* **2021**, *178*, 443–455. [[CrossRef](#)]
22. Fink, J.K.; Leibowitz, L. Thermodynamic and Transport Properties of Sodium Liquid and Vapor. 1995. Available online: <https://www.osti.gov/servlets/purl/94649> (accessed on 14 September 2022).
23. Tay, N.H.S.; Belusko, M.; Liu, M.; Bruno, F. Chapter 7—Static Concept at University of South Australia. In *High Temperature Thermal Storage Systems Using Phase Change Materials*; Cabeza, L., Tay, N., Eds.; Academic Press: Cambridge, MA, USA, 2018; pp. 157–191. [[CrossRef](#)]
24. Ereke, A.; Dincer, I. A New Approach to Energy and Exergy Analyses of Latent Heat Storage Unit. *Heat Transf. Eng.* **2009**, *30*, 506–515. [[CrossRef](#)]
25. Voller, V.R. Fast implicit finite-difference method for the analysis of phase change problems. *Numer. Heat Transf. Part B* **1990**, *17*, 155–169. [[CrossRef](#)]
26. Tehrani, S.S.M.; Shoraka, Y.; Diarce, G.; Taylor, R.A. An improved, generalized effective thermal conductivity method for rapid design of high temperature shell-and-tube latent heat thermal energy storage systems. *Renew. Energy* **2019**, *132*, 694–708. [[CrossRef](#)]
27. Carlson, M.D.; Middleton, B.M.; Ho, C.K. Techno-Economic Comparison of Solar-Driven sCO₂ Brayton Cycles Using Component Cost Models Baseline with Vendor Data and Estimates. In Proceedings of the ASME 2017 Power and Energy Conference, Charlotte, NC, USA, 25–30 June 2017. Available online: <https://www.osti.gov/servlets/purl/1427953> (accessed on 19 September 2022).
28. SMM. Sodium Price Charts. 2022. Available online: <https://www.metal.com/Other-Minor-Metals/201102250465> (accessed on 14 September 2022).
29. Nithyanandam, K.; Pitchumani, R. Optimization of an encapsulated phase change material thermal energy storage system. *Sol. Energy* **2014**, *107*, 770–788. [[CrossRef](#)]
30. Jacob, R.; Belusko, M.; Liu, M.; Saman, W.; Bruno, F. Using renewables coupled with thermal energy storage to reduce natural gas consumption in higher temperature commercial/industrial applications. *Renew. Energy* **2019**, *131*, 1035–1046. [[CrossRef](#)]
31. Jacob, R.; Belusko, M.; Inés Fernández, A.; Cabeza, L.F.; Saman, W.; Bruno, F. Embodied energy and cost of high temperature thermal energy storage systems for use with concentrated solar power plants. *Appl. Energy* **2016**, *180*, 586–597. [[CrossRef](#)]
32. Weiland, N.T.; Lance, B.W.; Pidaparti, S.R. sCO₂ Power Cycle Component Cost Correlations from DOE Data Spanning Multiple Scales and Applications. In Proceedings of the ASME Turbo Expo 2019, Phoenix, AZ, USA, 17–21 June 2019. Available online: <https://www.osti.gov/servlets/purl/1601743> (accessed on 19 September 2022).

33. Liang, T.; Vecchi, A.; Knobloch, K.; Sciacovelli, A.; Engelbrecht, K.; Li, Y.; Ding, Y. Key Components for Carnot Battery: Technology review, technical barriers and selection criteria. *Renew. Sustain. Rev.* **2022**, *163*, 112478. [[CrossRef](#)]
34. Peters, M.S.; Timmerhaus, K.D. *Plant Design and Economics for Chemical Engineers*; McGraw-Hill: New York, NY, USA, 1991.

Disclaimer/Publisher's Note: The statements, opinions and data contained in all publications are solely those of the individual author(s) and contributor(s) and not of MDPI and/or the editor(s). MDPI and/or the editor(s) disclaim responsibility for any injury to people or property resulting from any ideas, methods, instructions or products referred to in the content.